Advanced Composites and Hybrid Materials (2021) 4:696–706
https://doi.org/10.1007/s42114-021-00305-1

ORIGINAL RESEARCH

Polydopamine-coated chitosan hydrogel beads for synthesis and immobilization of silver nanoparticles to simultaneously enhance antimicrobial activity and adsorption kinetics

Taoran Wang[1] · Wusigale[1] · Deepa Kuttappan[2] · Mary Anne Amalaradjou[2] · Yaguang Luo[3] · Yangchao Luo[1]

Received: 31 May 2021 / Revised: 7 July 2021 / Accepted: 8 July 2021 / Published online: 27 July 2021

Abstract

In this study, the innovative and multi-functional chitosan-based hydrogel beads were immobilized with silver nanoparticles (AgNPs) via polydopamine coating to simultaneously enhance antimicrobial and adsorption activity. The morphological observation under scanning electron microscopy along with elemental mapping by energy disperse X-ray spectrometer indicated that AgNPs were successfully synthesized and immobilized not only on the surface but also the interior of PDA-coated chitosan beads. The covalent silver–carboxylate linkage along with hydrophobic and Van der Waals forces was evidenced by Fourier transform infrared spectroscopy to further confirm the *in situ* synthesis of AgNPs on the surface of beads. The equilibrium swelling rate of the prepared hydrogel beads decreased as pH increased, being 160%, 100%, and 80% at pH 5, 7, and 9, respectively. The adsorption performance of the hydrogel beads was investigated for the removal of an anionic dye and a metal ion (Cu (II)). The presence of AgNPs enhanced the adsorption capacity of the beads for the above-mentioned adsorbates. The antimicrobial activities were determined against potential human pathogens including Gram-negative *Escherichia coli* and Gram-positive *Staphylococcus aureus*. The antimicrobial activity of the obtained beads on the Gram-negative bacteria was higher than on the Gram-positive bacteria. The obtained hydrogel beads could be used for simultaneously controlling chemical and biological contaminants in wastewater.

Keywords Chitosan · Silver nanoparticles · Adsorption · Antimicrobial activity · Polydopamine · Water treatment

1 Introduction

Recently, intensive industrial and urban development, large population growth, and climate change have subjected water resources to severe pressure, from both quality and availability perspectives, increasing the need to find sustainable solutions to this compelling problem. One of the most promising practices to be explored is the reuse of wastewater. Wastewater reuse, also known as water recycling or water reclamation, reclaims water from a variety of sources then treats and reuses it for beneficial purposes such as agriculture and irrigation [1].

Depending on the source, wastewater could contain noxious dyes and heavy metal ions, as well as pathogenic microbes. Water reuse is not a new technique or concept; knowledge of wastewater treatment has been accumulated over the history of humankind. Thus far, a variety of wastewater treatment technologies have been developed include adsorption [2–4], membrane separation [5], chemical and biological degradation [6, 7], and electrochemical method [8]. Among them, physical adsorption is the most viable technology for wastewater management, due to its ease of operation with scalable facility for translational applications in industry. For several decades, activated carbons have been the most studied adsorbents as filtration devices for treating water to remove various types of chemical pollutants, particularly dyes and heavy metals [9, 10]. However, concerns

Taoran Wang and Wusigale contributed equally to this work

✉ Yangchao Luo
yangchao.luo@uconn.edu

[1] Department of Nutritional Sciences, University of Connecticut, 27 Manter Road, Storrs, CT 06269-4017, USA

[2] Department of Animal Science, University of Connecticut, Storrs, CT 06269, USA

[3] Food Quality, and Environmental Microbial and Food Safety Laboratories, USDA-ARS Beltsville Agricultural Research Center, Beltsville, MD 20705, USA

regarding their disadvantages such as high cost and inconsistent efficacy of carbons prepared from different sources have restricted their widespread applications in wastewater treatment [11]. Besides chemical pollutants, microbial contaminants including bacterial, viral, and protozoan pathogens have escalated the health hazards of untreated or improperly treated wastewater. Among various water disinfection methods, chlorination is the most widely used because it is inexpensive yet effective in disinfecting many microbial contaminants. However, chlorination can generate various disinfection byproducts, which may have severe harmful effect on water bodies [12, 13]. In order to remove both chemical and biological contaminants, traditional wastewater treatment technologies usually involve multiple-stage approaches, which are associated with high cost, poor efficiency, and require complicated processes and sophisticated maintenance [14]. Rapid population and economic growth has stimulated perpetually increasing demand for low-cost and high-efficiency wastewater treatment technologies. However, few studies have focused on the design of multifunctional wastewater treatment devices. Thus, it is expedient to explore simple and low-cost systems that can simultaneously control chemical quality and microbial safety of recycled wastewater.

Hydrogel is a three-dimensional (3D), flexible, and porous network of hydrophilic polymer chains that swell in water [15]. It has great potential in wastewater treatment due to its high adsorption capacity, rapid adsorption rate, and good reproducibility [16, 17]. Compared with traditional adsorbents (e.g., activated carbons), hydrogel can be more easily separated from water and reused. Chitosan, a derivative from chitin which is the second most abundant biopolymer in nature after cellulose, has a unique chemical structure, rich in reactive hydroxyl and amino groups, making it an excellent biomaterial for fabrication of hydrogel with high adsorption efficiency [16]. As a cationic biopolymer, chitosan exhibits intrinsic antimicrobial activity owing to its electrostatic interactions with negatively charged microbial cell membranes, which cause leakage of intracellular constituents [18–20]. To further enhance its adsorption and antimicrobial performance, several modification techniques like cross-linking, grafting, and combining with other materials have been reported [21]. Oxidized dextran (OD) is a dialdehyde polymer obtained from the oxidation of native dextran [22]. The abundant aldehyde groups on OD could react with amino groups of chitosan through Schiff base linkage to enhance the stability of chitosan hydrogel. Polydopamine (PDA), the final oxidation product of dopamine, has attracted much attention as versatile coatings that can be used to cover the surface of either organic or inorganic substrates with a conformal layer of adjustable thickness [23]. Silver nanoparticles (AgNPs) are well-known as the most universal antimicrobial substances due to their strong biocidal effect against microorganisms [24, 25]. Besides, AgNPs are also known for their anti-fungal, anti-inflammatory, and anti-viral properties, as well as electromagnetic properties [26–28]. In a recent study, Kodoth et al. synthesized AgNP-embedded pectin-based hydrogel as effective adsorbents for the removal of divalent metal ions and cationic dyes from aqueous solutions [29]. The presence of AgNPs was observed to enhance the adsorption capacity of the hydrogel, and the resultant hydrogel could absorb the maximum of 1950 mg/g crystal violet, 111 mg/g Cu(II), and 130 mg/g Pb(II). Chitosan/AgNP-bentonite prepared by ion-exchange method displayed a high antibacterial activity against *Staphylococcus aureus* (SA), with an inhibition zone with a diameter of about 35 mm [30].

In this study, we aimed at developing an innovative, simple, and multi-functional water treatment device to simultaneously control chemical property and microbial safety of recycled wastewater. The chitosan hydrogel beads, prepared using a coagulation technique, were first cross-linked and stabilized by OD via Schiff base linkage. To further enhance the disinfection performance, AgNPs were introduced on the surface of OD-crosslinked chitosan beads with the assistance of PDA. Specifically, the PDA coating, which was employed on the surface of OD-crosslinked chitosan beads, provided multiple sites for silver ion binding and phenolic hydroxyl structure for reduction of silver ions to AgNPs. Since it combines the excellent adsorption capability of chitosan hydrogel beads with the outstanding disinfection properties of AgNPs and chitosan, we hypothesized that the obtained water treatment device could simultaneously control chemical and biological contaminants in wastewater.

2 Materials and methods

2.1 Materials

Low molecular weight chitosan (75–85% deacetylated), sodium periodate ($NaIO_4$), dopamine hydrochloride, and Tris base were purchased from Sigma-Aldrich (St. Louis, MO, USA). Dextran (40 kDA) was obtained from Alfa Aesar (Ward Hill, MA, USA). Silver nitrate (0.25 N) was purchased from RICCA chemical company (Arlington, TX, USA). Hydrochloric acid (HCl), sodium hydroxide (NaOH), methanol, congo red, and copper sulfate ($CuSO_4$) were obtained from Fisher Scientific Co. (Norcross, GA, USA). Unless otherwise noted, all of the chemicals were of analytical grade and were used without further purification.

2.2 Preparation of OD cross-linked chitosan hydrogel beads

Chitosan solution (2%, w/v) was prepared by dissolving chitosan in 1% (v/v) acetic acid at room temperature overnight with gentle stirring for complete hydration. The chitosan solution was sonicated for 3 min before bead preparation to eliminate gas bubbles. Chitosan beads were prepared using

a Chemyx Fusion 4000 Syringe Pump (Stafford, TX, USA) to extrude chitosan solution dropwise through tubing connected to a 200-μL pipette tip and into a beaker containing coagulation solution (H_2O/methanol/NaOH = 4:5:1, w/w). The obtained chitosan beads were solidified in coagulation solution for 2 h while stirring at 150 rpm. Then, the alkaline solution was slowly decanted, and the chitosan beads were collected using filtration. The beads were successively washed with ultrapure water until the eluted water was neutral. Chitosan hydrogel beads were then directly added into a solution of OD to initiate the cross-linking via a Schiff base reaction between the amino groups of the chitosan and aldehyde groups of the OD for 24 h under gentle stirring. The OD was prepared as described previously [22]. The OD cross-linked chitosan beads were washed with ultrapure water to remove excessive OD. The obtained OD cross-linked chitosan beads were named OD-beads.

2.3 Preparation of AgNPs-PDA-coated chitosan hydrogel beads (Ag@beads)

Dopamine solution (2 mg/mL) was prepared by dissolving dopamine powder in Tris buffer (10 mM, pH 8.5). The OD-beads were soaked directly into the freshly prepared dopamine solutions under continuous stirring for 5 h at room temperature. After reaction, the products were taken out and washed with water until the rinse-water became clear. The chitosan hydrogel beads treated with dopamine were denoted as PDA-beads in the subsequent discussion. The PDA-beads were then immersed into $AgNO_3$ solution (50 mM) at room temperature for 6 h. The samples were rinsed with flowing water for 5 min and designated as Ag@beads in the subsequent discussion. The preparation procedure of Ag@beads is schematically shown in Fig. 1.

2.4 Characterization of Ag@beads

The prepared beads (chitosan beads, OD-beads, PDA-beads, Ag@beads) were placed on aluminum plates and dried in the oven for 2 h at 40 °C. After drying, the Fourier-transform infrared spectrophotometry (FTIR, NicoletTM iSTM5, Thermo Scientific, Waltham, MA, USA) was used to study the interaction between coating materials and chitosan. The FTIR spectra of dried beads were measured in the range of 500–4000 cm^{-1}. The results were analyzed using OMNIC software, version 8.0.

For scanning electron microscope (SEM) observation, the oven-dried bead samples were placed on double-sided carbon tape. Before observation by SEM (JSM-6335F, JEOL Ltd., Tokyo, Japan), all of the samples were coated with gold using a sputter coater. The chemical composition of samples' surface and intersection was determined by energy dispersive x-ray spectroscopy (EDS, X-Max 80 Silicon Drift Detector, Oxford Instruments, UK).

The swelling rate of Ag@beads was measured under phosphate-buffered saline (PBS) at pH 5, 7, and 9. The oven-dried Ag@beads were immersed into PBS at 37 °C for 6 h. During incubation, the Ag@beads were taken out from the PBS at predetermined time points, 1, 2, 3, 4, 5, and 6 h, and the surface fluids were carefully and completely removed by filter paper before weighing. The swelling rate was calculated based on the following equation:

$$\text{Swelling rate } (\%) = \frac{W_S - W_D}{W_D} \times 100$$

Here, W_s and W_D represent the weight of dried Ag@beads and the weight of Ag@beads after swelling in PBS, respectively. The swelling rate is defined as the fractional increase in the weight of the hydrogel due to water absorption.

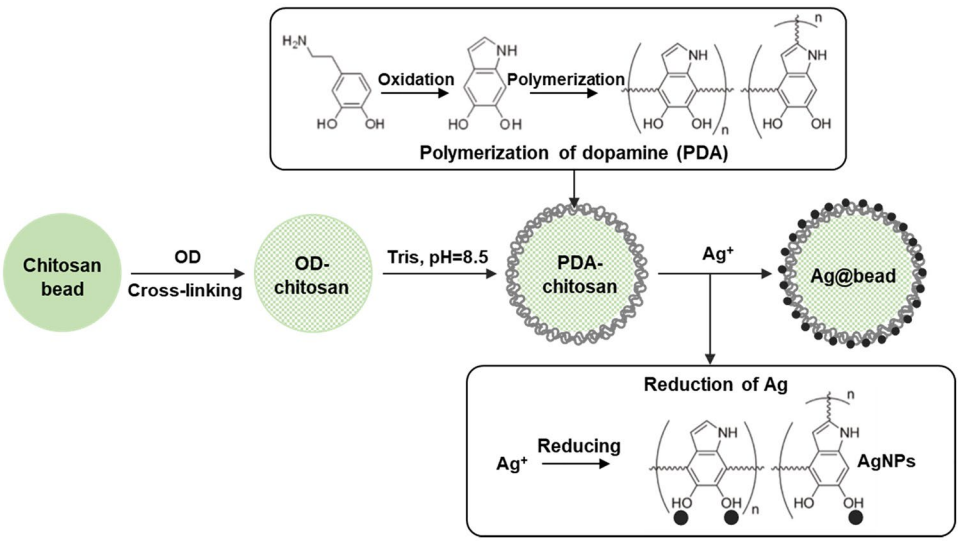

Fig. 1 Schematic diagram of the preparation of the Ag@beads

2.5 Adsorption studies

A solution of congo red (CR) was prepared in water at concentration of 1 mg/mL, and experimental solutions of CR concentrations were obtained by successive dilutions. The concentration of CR in experimental solution was determined from the calibration curve prepared by measuring absorbance of different predetermined concentrations of CR solutions at 497 nm using UV/Vis spectroscopy. Cu (II) ion stock solution (1 mg/mL) was prepared and diluted to give the appropriate concentrations.

The adsorption study was carried out in a water bath shaker at 150 rpm and 30 °C using 20-mL glass vials containing 0.2 g of hydrated Ag@beads or chitosan beads as control and 10 mL of CR or Cu (II) solutions of pH 5 at 0.5 mg/mL concentration. Different time intervals of up to 8 h were used for this study. The residual CR concentration in the experimental solution at each predetermined time point was analyzed using a UV/Vis spectrophotometer at 497 nm. The residual Cu (II) ions were analyzed at a wavelength of 325 nm using an inductively coupled plasma spectrometer (ICPMS). The amount of CR or Cu (II) ions adsorbed (mg/g) was calculated based on the following mass balance equation:

$$q_t(mg/g) = \frac{(C_0 - C_t)}{W} \times V$$

Here, q_t is the amount of CR or Cu (II) ions adsorbed on the beads at a predetermined time per gram dry weight of the adsorbent, mg/g; C_0 is the initial concentration of CR or Cu (II) in the solution, mg/L; C_t is the concentration of CR or Cu (II) in the solution at time t, mg/L; V is the volume of the solution, L; and W is the weight of the hydrogel beads, g.

An elemental analysis of the samples before and after adsorption was performed by EDS (X-Max 80 Silicon Drift Detector, Oxford Instruments, UK).

2.6 Antibacterial studies

The antimicrobial efficacy of Ag@beads was evaluated against *Escherichia coli* ATCC *BAA 2196* (EC) and *Staphylococcus aureus* ATCC 12600 (SA). All bacteriological media used in the study were procured from Difco (Difco Becton, MD, USA). EC and SA were grown in tryptic soy broth (TSB) at 37 °C overnight. After incubation, the cultures were centrifuged (3000 ×g, 12 min, 4 ºC) and washed twice with phosphate-buffered saline (PBS; pH 7.0). The pellet was then resuspended in PBS and used as the inoculum. Bacterial counts were confirmed following serial dilution and plating on Tryptic Soy agar (TSA). The hydrogel bead samples were soaked and washed with sterilized ultrapure water for 24 h to remove any existing bacteria, and then the beads were plated on TSA to verify absence of any bacterial growth. The antibacterial activity of the Ag@beads was tested at two (0.2 and 0.5 g/mL) and at two temperatures [optimum (37°C) and ambient (24°C)]. The washed overnight culture was appropriately diluted in TSB to obtain an inoculum of 10^6 CFU/mL. This resuspended culture was then treated with the specified concentrations of Ag@beads and incubated at their respective temperatures with continuous shaking for 24 h. Another batch of inoculum that was not exposed to the Ag@beads (control) was also included in the study. At different intervals (0, 1.5, 3, 6, 12, and 24 h), the surviving bacterial population was determined by dilution and plating on TSA [31]. The assay for each bacterial species and treatment was run in duplicate, and the entire experiment was repeated three times.

2.7 Statistical analysis

All of the results were presented as the mean ± standard deviation (SD) of at least triplicate determinations. The data were analyzed using one-way analysis of variance (ANOVA) with Tukey's multiple-comparison test to compare the significance among the samples. The p was set at 0.05. For the antibacterial assay, *bacterial* counts at different time periods were log transformed and tested for significance at a p value of <0.05 using the PROC GLIMMIX procedure of SAS (version 9.2; SAS Institute Inc., Cary, NC).

3 Results and discussion

3.1 Physicochemical characterization

3.1.1 Morphological observation

The digital photographs of freshly prepared chitosan beads, PDA-beads, and Ag@beads are shown in Fig. 2A, B, and C, respectively. As evident from the photographs, the beads were spherical in shape with approximate diameter of 2.5 mm. The prepared chitosan beads were pearl white in appearance (Fig. 2A). Upon PDA surface functionalization, the PDA-beads turned brown in color (Fig. 2B) and ultimately dark brown after immobilization of silver nanoparticles (Ag@beads: Fig. 2C). Based on previous literature, the polymerization of dopamine and formation of PDA is initiated through a solution oxidation method under basic conditions, during which the oxygen serves as an oxidant and dopamine serves as the monomeric unit that can be oxidized and spontaneously self-polymerized [32]. Thus, the obtained PDA-beads exhibited a typical brownish color due to the presence of PDA [33]. After reduction of $AgNO_3$, the Ag@beads showed a dark brown color, indicating the synthesis of silver nanoparticles [34]. The morphology and

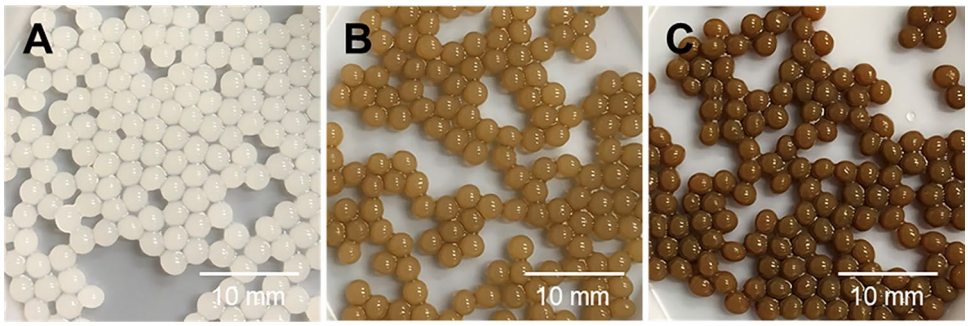

Fig. 2 Digital photos of (**A**) chitosan beads; (**B**) PDA-beads; and (**C**) Ag@beads

surface details of the oven-dried beads were then viewed under SEM (Fig. 3). As can be seen from Fig. 3A, the dried chitosan beads had an oval shape with smooth surface, while the Ag@beads exhibited a more robust polymer network and spherical shape with a diameter of about 600 µm and could free-stand after drying (Fig. 3D). A smooth and uniform surface morphology was observed for the chitosan beads (Fig. 3B), while the surface of the Ag@beads was relatively rough and covered with particles/granules of sizes ranging from 50 nm to several hundred nanometers (Fig. 3E), which was similar to AgNPs observed in previous studies [35, 36]. Figure 3C and F show the cross-sectional morphology of chitosan beads and Ag@beads. The chitosan beads presented a typical hydrogel morphology with porous and highly networked structure (Fig. 3C). After modifications, the Ag@beads maintained the hydrogel porous structure of chitosan beads, and many nano-sized particles were observed that were well dispersed in the polymer matrix (Fig. 3F). The presence of those particles could be caused by diffusion of AgNPs from the surface to the interior of the hydrogel beads. EDS spectra of the Ag@beads were recorded to further confirm the presence of AgNPs within the system (Fig. 4). The EDS results showed that the AgNPs were uniformly distributed over the entire surface as well as embedded inside of the Ag@beads as can be seen from the cross-sectional view. Therefore, it was concluded that PDA was capable of reducing silver ions to AgNPs and the AgNPs were able to migrate into the hydrogel beads.

3.1.2 FTIR analysis

To study the possible interactions between chitosan and other components in the formation of the Ag@beads, FTIR spectroscopy was employed to monitor the transformation of the chemical bonds in chitosan, OD-chitosan, PDA-chitosan, and Ag@beads, as exhibited in Fig. 5. Chitosan beads showed the typical bands of chitosan polymer, a typical spectrum with three characteristic peaks at 3357, 1653, and 1590 cm^{-1},

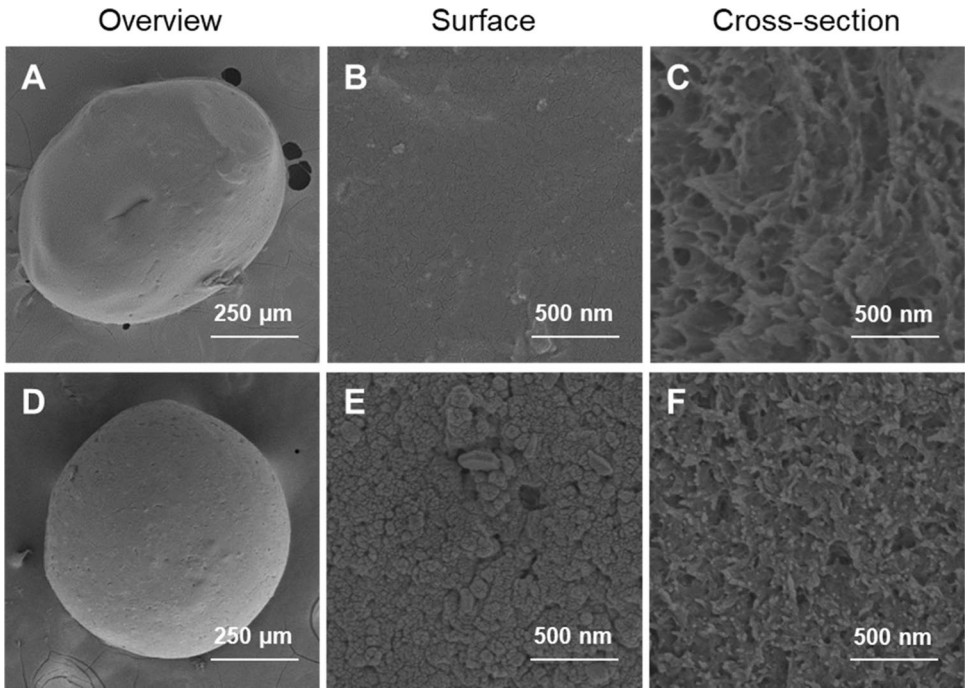

Fig. 3 SEM images of chitosan beads and Ag@beads. Overview of chitosan beads (**A**) and Ag@beads (**D**). Surface morphology of chitosan beads (**B**) and Ag@beads (**E**). Cross-sectional view of beads from chitosan beads (**C**) and Ag@beads (**F**)

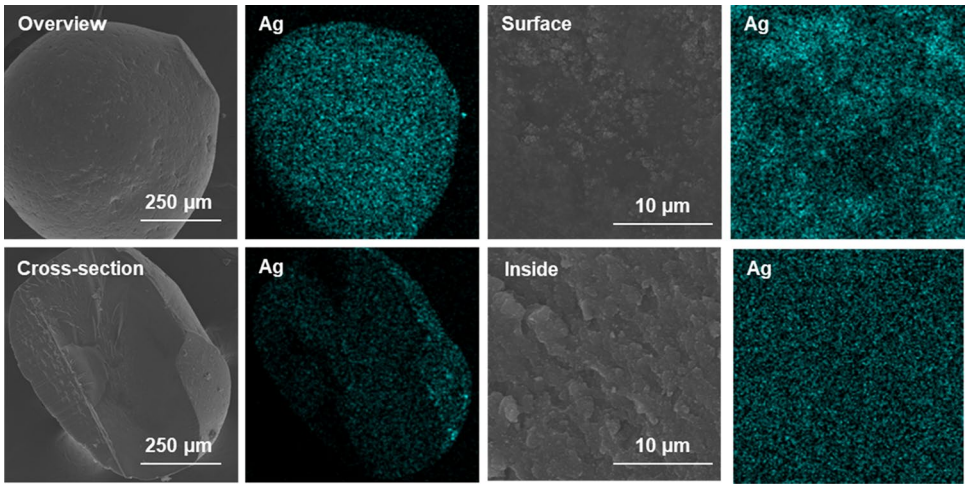

Fig. 4 EDS results of Ag@ beads

being O–H stretching, C=O stretching from amide I, N–H bending, and C–N stretching from amide II, respectively [37] (Fig. 5A). After crosslinking with OD, the absorption peaks corresponding to imine bonds appeared at 1613–1631 cm^{-1}, which were caused by the reaction occurring between the amino groups of the chitosan and the aldehyde groups of the OD. However, it is difficult to identify this peak in the spectra of the OD-chitosan beads, which might be obscured by the overlay of the imine bond with the amide bond from chitosan [38] (Fig. 5B). After adsorption of the PDA coating, the FTIR spectrum of the hydrogel beads exhibited some characteristic peaks of PDA at 1600 cm^{-1} and 1504 cm^{-1} corresponding to the C=C resonance vibration of the aromatic group [39]. However, both of them overlapped with the peak at 1644 cm^{-1} (C=O stretching from amide I in chitosan) (Fig. 5C). Upon the reduction of silver ions into nanoparticles, the C=O stretching bands at about 1644 cm^{-1} shifted to 1636 cm^{-1} accompanied by a decrease in intensity in the case of Ag@beads (Fig. 5D). These changes suggest the existence of a covalent link between carboxylic anions and silver ions, forming silver–carboxylate bonds that might interact with the polymeric backbone chains through hydrophobic and Van der Waals forces [40]. Simultaneously, the absorption band at 3350 cm^{-1} shifted to 3272 cm^{-1}, possibly indicating that AgNPs bind to the –OH groups and are stabilized by hydrogen bonding in the hydrogel matrices [41].

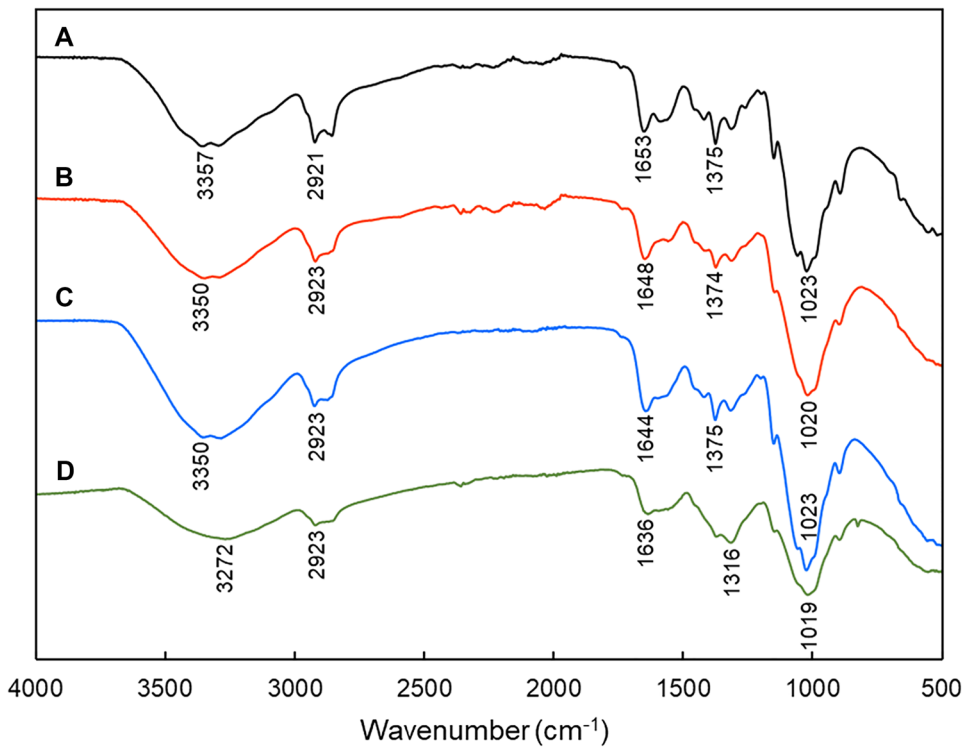

Fig. 5 FTIR spectra of (**A**) chitosan; (**B**) OD-chitosan; (**C**) PDA-chitosan; and (**D**) Ag@ beads

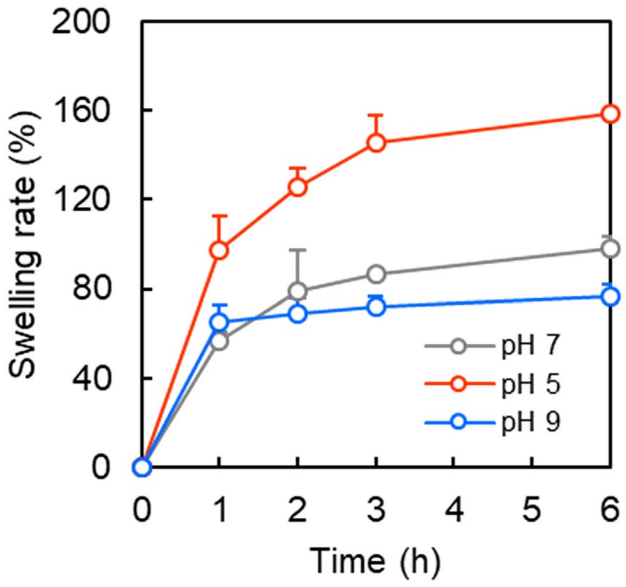

Fig. 6 Swelling test results of Ag@beads under different pHs

3.2 Swelling behavior

The swelling behavior of Ag@beads at different pHs is shown in Fig. 6. Within the first 1 h, the hydrogel beads displayed rapid swelling, and then gradually reached an equilibrium value of 160%, 100%, and 80%, which was observed after 3, 2, and 1 h for pH 5, 7, and 9, respectively. Swelling occurs when water molecules are absorbed by the hydrogel beads. Initially, the water molecules form hydrogen bonds with hydrophilic functional groups (e.g., hydroxyl groups) present in the polymer chains of chitosan. As swelling progresses, more water molecules become orientated around bound water to form network-like structures or clusters. Finally, excess water enters freely into the gel network resulting in a greater degree of swelling [42]. The equilibrium swelling rate of Ag@beads decreased as pH increased from 5 to 9, which is consistent with findings in previous studies [43, 44]. Such swelling behavior has been attributed to the changes in gel structure in acidic medium brought about by the protonation of chitosan amino groups, which leads to the dissociation of the hydrogen bonding between amino and other groups within Ag@beads [44]. A previous study reported that as the pH increased from 4 to 9, the swelling rate of bare chitosan beads decreased from 468% to 247% [43], which showed higher swelling capacity as compared to Ag@beads. This might be due to the fact that binding of AgNPs with functional groups of chitosan resulting in highly cross-linked structure which in turn lowers its swelling capacity and water absorption ability [45].

3.3 Adsorption properties

Adsorption experiments using organic dye (i.e., CR) and heavy metal (i.e., Cu (II)) were carried out to determine the adsorption capacity of Ag@beads with chitosan hydrogel beads functioning as a control. The adsorption kinetics of CR (A) and Cu (II) (B) in solution with an initial concentration of 200 ppm by the Ag@beads and chitosan hydrogel beads are illustrated in Fig. 7. The adsorption of CR on chitosan beads and Ag@beads was rapidly increased through the first 4 h, and then the adsorption capacity at equilibrium state was reached at about 4 and 7 mg/g, respectively, as displayed in Fig. 7A. As shown in Fig. 7B, the adsorption of Cu (II) on chitosan beads and Ag@beads increased sharply within the first 1 h and then slowly increased until 6 h. The adsorption capacity at equilibrium state was reached at 7 and 9 mg/g, respectively. The rapid adsorption in the initial stage was ascribed to the film formation on the exterior surface of hydrogel network, while the following slow adsorption process was due to the intraparticle diffusion process [46].

To further confirm the adsorption capacity of hydrogel beads, EDS was used to detect the S and Cu (II) originating from CR and $CuSO_4$, respectively. As shown in Fig. 8, the Ag@beads (3.27 ± 0.81%) exhibited significantly higher surface S content compared to chitosan beads (1.88 ± 0.24%), indicating higher CR adsorption efficacy. Similarly, a significantly higher Cu (II) content in Ag@beads (8.09

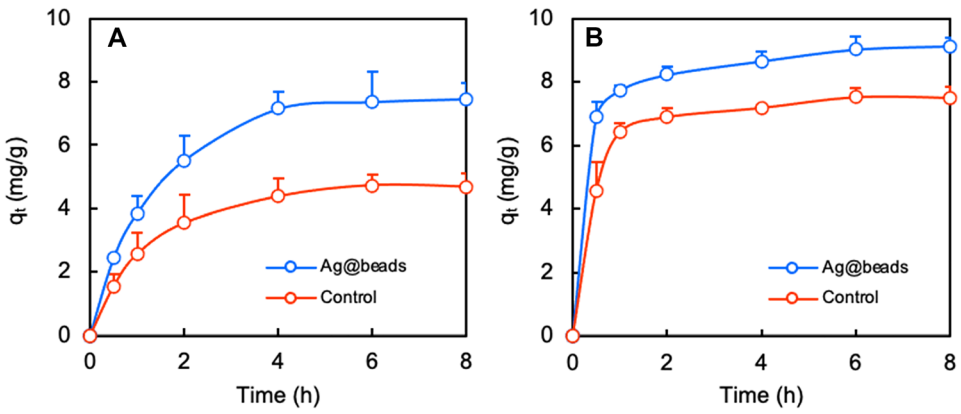

Fig. 7 Plots of q_t *vs.* contact time for CR (**A**) and Cu (II) (**B**) adsorption onto the chitosan beads (control) and Ag@beads. Initial CR and Cu (II) concentration: 200 ppm

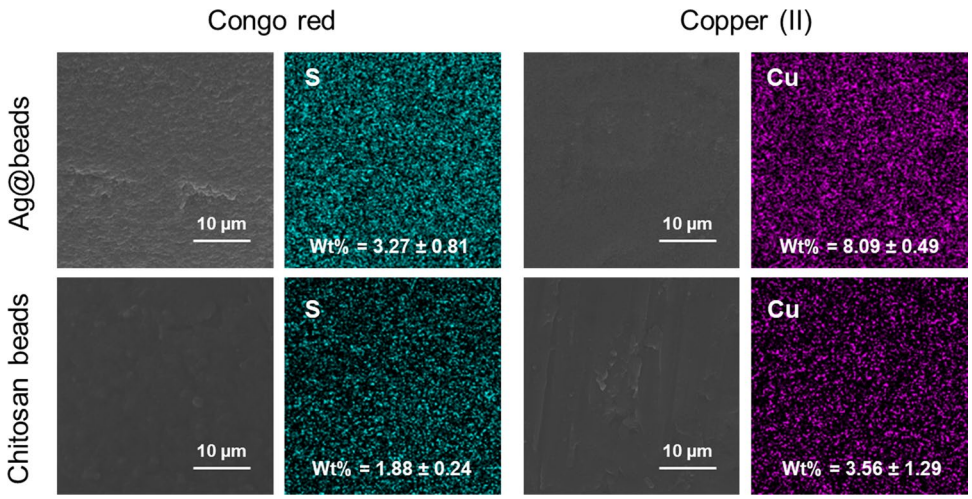

Fig. 8 EDS results of Ag@beads and chitosan beads surface after adsorption

± 0.49%) was detected after the $CuSO_4$ absorption test in comparison to chitosan beads (3.56 ± 1.29). In summary, the presence of PDA and silver nanoparticle layers could significantly increase the adsorption capacity of hydrogel beads. It is well known that chitosan hydrogel beads are regarded as a potential adsorbent for effective removal of dyes and heavy metals in wastewater treatment due to the presence of abundant amino ($–NH_2$) and hydroxyl (–OH) groups, as well as a highly connected network structure [47–49]. The immobilization of AgNPs resulted in significantly enhanced adsorption capacity and performance of Ag@beads for CR and Cu (II) due to ion exchange and metal complexation mechanisms [21, 50]. The ion exchange mechanism might occur as Cu (II) substitutes the silver ions in hydrogel beads. The metal complexation mechanism may occur via the coordination of the $–NH_2$ and –OH groups of chitosan with Cu (II). Each of amino group's nitrogen as well as hydroxyl group's oxygen has a pair of electrons, which could be accepted by metal cation. It has been reported that the ability of amino group's nitrogen to donate its electron is stronger than the hydroxyl group's oxygen [51].

3.4 Antibacterial assessment

The antibacterial performance of Ag@beads against EC and SA at two dosages of 0.2 and 0.5 g beads in 1 mL of bacterial culture at 37 °C and room temperature is shown in Fig. 9. Untreated bacteria (control) grew from ~6 log CFU/mL to 9 log CFU/mL by the end of the 24-h incubation at 37 °C (Fig. 9A and B) and room temperature (Fig. 9C and D). At 37 °C, Ag@beads at 0.2 and 0.5 g could completely inhibit EC after 12 and 1.5 h of incubation, respectively (Fig. 9A). However with SA, exposure to Ag@beads (0.2 and 0.5 g/mL) did not result in a complete inactivation. However, when compared to the control, Ag@beads resulted in greater than 6 log reduction in SA population (Fig. 9B). At room temperature, 0.2 g of Ag@beads treatment reduced EC populations to 4.5 log CFU/mL after 24 h, whereas Ag@beads at 0.5 g could completely inhibit EC after 6 h (Fig. 9C). Exposure to 0.2 g beads resulted in a bacteriostatic effect on SA with no significant increase in population at the end of the 24-h study, while 0.5 g of beads was sufficient to decrease bacterial number to 4 log CFU/mL at the end of the study (Fig. 9D). In both cases, approximately 9 log CFU/mL of SA was recovered from the control samples at room temperature. Considering that the chitosan beads, OD-beads, and PDA-beads showed no antibacterial activity (data not shown), antibacterial activity was directly related to the AgNPs and silver ions. It has been proposed that the antibacterial mechanisms of AgNPs and silver ions include cell wall and membrane damage, intracellular penetration and damage, and oxidative stress [52, 53].

The antimicrobial activity on the Gram-negative bacteria (EC: Fig. 9A and C) was slightly higher than that on the Gram-positive bacteria (SA: Fig. 9B and D), in agreement with previous studies on silver and chitosan-silver composites [54]. It has been reported that the minimum inhibitory concentrations (MICs) of AgNPs with the particle size of 13.5 nm at 37 °C were 6.6 and 33 nM for *Escherichia coli* ATCC 43886 and *Staphylococcus aureus* ATCC 19636, respectively [55]. Another study indicated that the MIC of myramisin-capped AgNPs with the particle size of 10 nm at 37 °C was < 1 and 5 μg/mL for *Escherichia coli* ATCC 25922 and *Staphylococcus aureus* FDA 209P, respectively [56]. The peptidoglycan layer in the Gram-positive bacterial cell wall provides a natural barrier which prevents penetration of the nanoparticles, while Gram-negative bacteria have thinner cell wall and less peptidoglycan [53, 55]. Moreover, the antibacterial activity of Ag@beads was more effective at 37 °C (Fig. 9A and B) than at room temperature (Fig. 9C and D). A number of studies have revealed that the silver ions released from AgNPs have inhibitory effects by targeting a

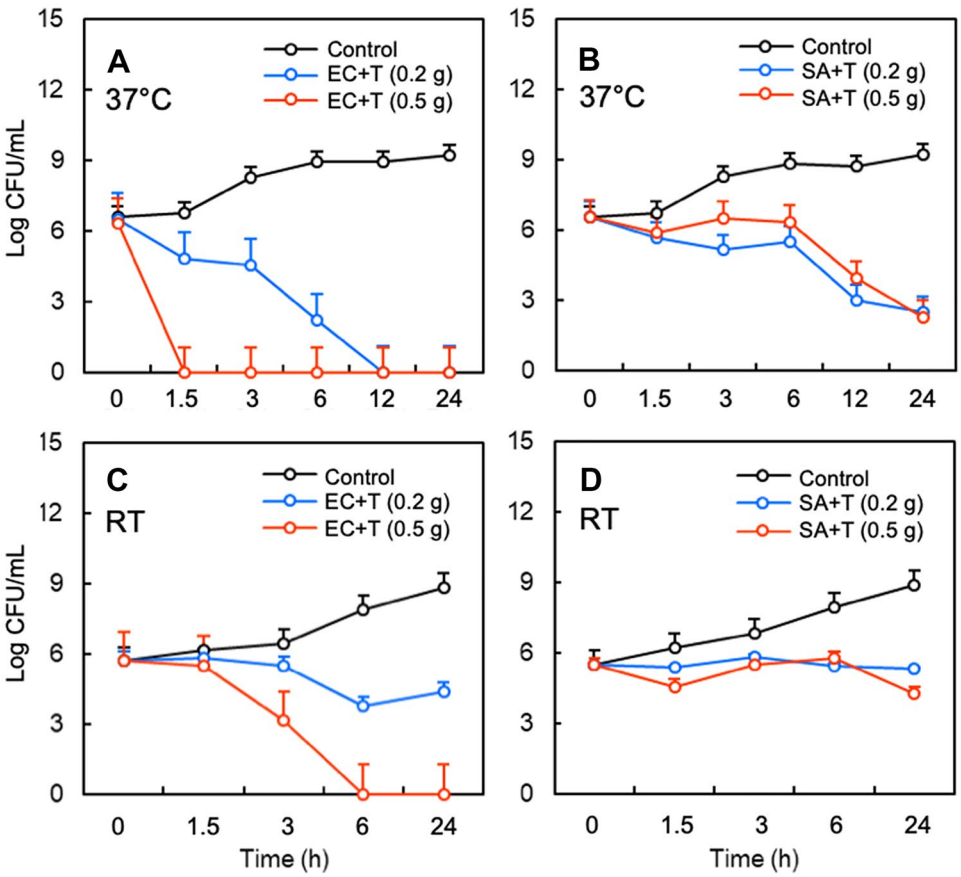

Fig. 9 Antimicrobial activity of Ag@beads against *Escherichia coli* (*E. coli, EC*) and *Staphylococcus aureus* (*S. aureus, SA*) at two dosages of 0.2 and 0.5 g beads in 1 mL of bacterial culture under 37°C (**A** and **B**) and room temperature (24°C; **C** and **D**). T refers to the treatment with Ag@beads, and control sample is untreated bacteria. RT: room temperature

broad spectrum of microorganisms [57–59], and silver ions release rates increase with temperature in the range 0–37 °C [60]. Therefore, the Ag@beads exhibited strong antibacterial property, owing to the AgNP contribution.

4 Conclusions

In conclusion, the results of this study suggest that the chitosan hydrogel beads can be successfully immobilized with AgNPs with the assistance of a PDA coating after crosslinking with OD in order to simultaneously enhance antimicrobial and adsorption activity. The obtained fresh Ag@beads exhibited dark brown color and spherical shape with an average size of 2.5 mm, and the dried beads had a size of about 600 µm. The prepared hydrogel beads showed pH sensitivity with the highest swelling degree at low pH, probably because the protonation of chitosan amino groups caused the dissociation of hydrogen bonds between amino and other groups within Ag@beads. Moreover, the results of dye and metal adsorption studies showed that AgNPs improved the adsorption performance of the chitosan hydrogel beads through ion exchange and metal complexation mechanisms. In addition, the Ag@beads exhibited strong antibacterial activity, owing to the AgNP contribution, and exhibited higher antibacterial activity against Gram-negative bacteria than Gram-positive bacteria. Therefore, Ag@beads are good candidates to employ in an integrative approach to efficiently control both the microbial and chemical quality of wastewater. More studies on their cytotoxicity and environmental toxicity are required to accurately assess their impact on the environment and public health.

Funding This work was, in part, supported by the U.S. Department of Agriculture (USDA), National Institute of Food and Agriculture, Specialty Crop Research Initiative, Award No. 2016-51181-25403, and Hatch Multistate project accession number 1020207.

Declarations

Conflict of interest The authors declare no competing interests.

References

1. Asano T, Burton F, Leverenz H (2007) Water reuse: issues, technologies, and applications. McGraw-Hill Education.
2. Aivalioti M, Papoulias P, Kousaiti A, Gidarakos E (2012) Adsorption of BTEX, MTBE and TAME on natural and modified diatomite. J Hazard Mater 207:117–127. https://doi.org/10.1016/j.jhazmat.2011.03.040

3. Bandura L, Kołodyńska D, Franus W (2017) Adsorption of BTX from aqueous solutions by Na-P1 zeolite obtained from fly ash. Process Saf Environ 109:214–223. https://doi.org/10.1016/j.psep.2017.03.036
4. Alqadami AA, Naushad M, Abdalla MA, Ahamad T, AlOthman ZA, Alshehri SM, Ghfar AA (2017) Efficient removal of toxic metal ions from wastewater using a recyclable nanocomposite: a study of adsorption parameters and interaction mechanism. J Clean Prod 156:426–436. https://doi.org/10.1016/j.jclepro.2017.04.085
5. Giacobbo A, Meneguzzi A, Bernardes AM, de Pinho MN (2017) Pressure-driven membrane processes for the recovery of antioxidant compounds from winery effluents. J Clean Prod 155:172–178. https://doi.org/10.1016/j.jclepro.2016.07.033
6. Jin X, Yu B, Lin J, Chen Z (2016) Integration of biodegradation and nano-oxidation for removal of PAHs from aqueous solution. ACS Sustain. Chem Eng 4(9):4717–4723. https://doi.org/10.1021/acssuschemeng.6b00933
7. Yamaga F, Washio K, Morikawa M (2010) Sustainable biodegradation of phenol by Acinetobacter calcoaceticus P23 isolated from the rhizosphere of duckweed Lemna aoukikusa. Environ Sci Technol 44(16):6470–6474. https://doi.org/10.1021/es1007017
8. Gatsios E, Hahladakis JN, Gidarakos E (2015) Optimization of electrocoagulation (EC) process for the purification of a real industrial wastewater from toxic metals. J Environ Manage 154:117–127. https://doi.org/10.1016/j.jenvman.2015.02.018
9. Kobya M, Demirbas E, Senturk E, Ince M (2005) Adsorption of heavy metal ions from aqueous solutions by activated carbon prepared from apricot stone. Bioresour Technol 96(13):1518–1521. https://doi.org/10.1016/j.biortech.2004.12.005
10. Gupta VK, Srivastava SK, Mohan D, Sharma S (1998) Design parameters for fixed bed reactors of activated carbon developed from fertilizer waste for the removal of some heavy metal ions. Waste Manage 17(8):517–522. https://doi.org/10.1016/S0956-053X(97)10062-9
11. Foo KY, Hameed BH (2010) An overview of dye removal via activated carbon adsorption process. Desalination Water Treat. 19(1–3):255–274. https://doi.org/10.1016/j.biortech.2004.12.005
12. Nieuwenhuijsen MJ, Toledano MB, Eaton NE, Fawell J, Elliott P (2000) Chlorination disinfection byproducts in water and their association with adverse reproductive outcomes: a review. Occup Environ Med 57(2):73–85. https://doi.org/10.1136/oem.57.2.73
13. Jolley RL, Brungs WA, Cotruvo JA, Cumming RB, Mattice JS, Jacobs VA (1983) Water chlorination: environmental impact and health effects. Volume 4, Book 1. Chemistry and water treatment, Ann Arbor Science Publishers, Ann Arbor, MI
14. Centers for Disease Control and Prevention (1999) Ten great public health achievements–United States, 1900–1999. MMWR. Morbidity and mortality weekly report 48(12):241–243
15. Ahmed EM (2015) Hydrogel: Preparation, characterization, and applications: a review. J Adv Res 6(2):105–121. https://doi.org/10.1016/j.jare.2013.07.006
16. Pakdel PM, Peighambardoust SJ (2018) Review on recent progress in chitosan-based hydrogels for wastewater treatment application. Carbohydr Polym 201:264–279. https://doi.org/10.1016/j.carbpol.2018.08.070
17. Van Tran V, Park D, Lee YC (2018) Hydrogel applications for adsorption of contaminants in water and wastewater treatment. Environ Sci Pollut Res 25(25):24569–24599. https://doi.org/10.1007/s11356-018-2605-y
18. Goy RC, Britto DD, Assis OB (2009) A review of the antimicrobial activity of chitosan. Polímeros 19(3):241–247. https://doi.org/10.1590/S0104-14282009000300013
19. Devlieghere F, Vermeulen A, Debevere J (2004) Chitosan: antimicrobial activity, interactions with food components and applicability as a coating on fruit and vegetables. Food Microbiol 21(6):703–714. https://doi.org/10.1016/j.fm.2004.02.008
20. Qu B, Luo Y (2020) Chitosan-based hydrogel beads: preparations, modifications and applications in food and agriculture sectors - a review. Int J Biol Macromol 152:437–448. https://doi.org/10.1016/j.ijbiomac.2020.02.240
21. Upadhyay U, Sreedhar I, Singh SA, Patel CM, Anitha KL (2021) Recent advances in heavy metal removal by chitosan based adsorbents. Carbohydr Polym 251:117000. https://doi.org/10.1016/j.carbpol.2020.117000
22. Wang T, Hu Q, Lee JY, Luo Y (2018) Solid lipid–polymer hybrid nanoparticles by in situ conjugation for oral delivery of astaxanthin. J Agric Food Chem. 66(36):9473-9480. https://doi.org/10.1021/acs.jafc.8b02827
23. Ball V (2018) Polydopamine nanomaterials: recent advances in synthesis methods and applications. Front Bioeng Biotechnol 6:109. https://doi.org/10.3389/fbioe.2018.00109
24. Baker C, Pradhan A, Pakstis L, Pochan DJ, Shah SI (2005) Synthesis and antibacterial properties of silver nanoparticles. J Nanosci Nanotechnol 5(2):244–249. https://doi.org/10.1166/jnn.2005.034
25. Franci G, Falanga A, Galdiero S, Palomba L, Rai M, Morelli G, Galdiero M (2015) Silver nanoparticles as potential antibacterial agents. Molecules 20(5):8856–8874. https://doi.org/10.3390/molecules20058856
26. Govindappa M, Farheen H, Chandrappa CP, Rai RV, Raghavendra VB (2016) Mycosynthesis of silver nanoparticles using extract of endophytic fungi, Penicillium species of Glycosmis mauritiana, and its antioxidant, antimicrobial, anti-inflammatory and tyrokinase inhibitory activity. Adv Nat Sci- Nanosci Nanotechnol 7(3):035014. https://doi.org/10.1088/2043-6262/7/3/035014
27. Xie P, Liu Y, Feng M, Niu M, Liu C, Wu N, Sui K, Patil RR, Pan D, Guo Z, Fan R (2021) Hierarchically porous Co/C nanocomposites for ultralight high-performance microwave absorption. Adv Compos Hybrid Mater 4(1):173–185
28. Wu N, Du W, Hu Q, Jiang SV (2021) Recent development in fabrication of Co nanostructures and their carbon nanocomposites for electromagnetic wave absorption. Eng Sci 13:11-23. https://doi.org/10.30919/es8d1149
29. Kodoth AK, Badalamoole V (2020) Silver nanoparticle-embedded pectin-based hydrogel for adsorptive removal of dyes and metal ions. Polym Bull 77(2):541–564. https://doi.org/10.1007/s00289-019-02757-4
30. Abdelkrim S, Mokhtar A, Djelad A, Bennabi F, Souna A, Benguedda A, Sassi M (2020) Chitosan/Ag-bentonite nanocomposites: preparation, characterization, swelling and biological properties. J Inorg Organomet Polym Mater 30(3):831–840. https://doi.org/10.1007/s10904-019-01219-8
31. Narayanan A, Nair MS, Muyyarikkandy MS, Amalaradjou MA (2018) Inhibition and inactivation of uropathogenic Escherichia coli biofilms on urinary catheters by sodium selenite. Int J Mol Sci 19(6). https://doi.org/10.3390/ijms19061703
32. Qiu Y, Zhu Z, Miao Y, Zhang P, Jia X, Liu Z, Zhao X (2020) Polymerization of dopamine accompanying its coupling to induce self-assembly of block copolymer and application in drug delivery. Polym Chem 11(16):2811–2821. https://doi.org/10.1039/D0PY00085J
33. Bucher T, Clodt JI, Grabowski A, Hein M, Filiz V (2017) Colour-value based method for polydopamine coating-stability characterization on polyethersulfone membranes. Membranes 7(4):70. https://doi.org/10.3390/membranes7040070
34. Azizi S, Namvar F, Mahdavi M, Ahmad MB, Mohamad R (2013) Biosynthesis of silver nanoparticles using brown marine macroalga. Sargassum muticum aqueous extract. Materials 6(12):5942–5950. https://doi.org/10.3390/ma6125942

35. Bhagat M, Anand R, Datt R, Gupta V, Arya S (2019) Green synthesis of silver nanoparticles using aqueous extract of Rosa brunonii Lindl and their morphological, biological and photocatalytic characterizations. J Inorg Organomet Polym Mater 29(3):1039–1047. https://doi.org/10.1007/s10904-018-0994-5
36. Vona D, Cicco SR, Ragni R, Leone G, Presti ML, Farinola GM (2018) Biosilica/polydopamine/silver nanoparticles composites: new hybrid multifunctional heterostructures obtained by chemical modification of Thalassiosira weissflogii silica shells. MRS Commun 8(3):911–917. https://doi.org/10.1557/mrc.2018.103
37. Luo Y, Teng Z, Li Y, Wang Q (2015) Solid lipid nanoparticles for oral drug delivery: chitosan coating improves stability, controlled delivery, mucoadhesion and cellular uptake. Carbohydr Polym 122:221–229. https://doi.org/10.1016/j.carbpol.2014.12.084
38. Wang T, Luo Y (2018) Chitosan hydrogel beads functionalized with thymol-loaded solid lipid-polymer hybrid nanoparticles. Int J Mol Sci 19(10):3112. https://doi.org/10.3390/ijms19103112
39. Ma X, Wu G, Dai F, Li D, Li H, Zhang L, Deng H (2021), Chitosan/polydopamine layer by layer self-assembled silk fibroin nanofibers for biomedical applications. Carbohydr Polym 251:110758. https://doi.org/10.1016/j.carbpol.2020.117058
40. Ngoc-Thang N, Liu J-H (2014) A green method for in situ synthesis of poly(vinyl alcohol)/chitosan hydrogel thin films with entrapped silver nanoparticles. J Taiwan Inst Chem Eng 45(5):2827–2833. https://doi.org/10.1016/j.jtice.2014.06.017
41. Nesovic K et al (2019) Chitosan-based hydrogel wound dressings with electrochemically incorporated silver nanoparticles - in vitro study. Eur Polym J 121:109257. https://doi.org/10.1016/j.eurpolymj.2019.109257
42. Qu X, Wirsen A, Albertsson AC (2000) Novel pH-sensitive chitosan hydrogels: swelling behavior and states of water. Polymer 41(12):4589–4598. https://doi.org/10.1016/S0032-3861(99)00685-0
43. El-Hady A, Saeed S (2020) Antibacterial properties and pH sensitive swelling of insitu formed silver-curcumin nanocomposite based chitosan hydrogel. Polymers 12(11):2451. https://doi.org/10.3390/polym12112451
44. Yao KD et al (1994) Swelling kinetics and release characteristic of cross-linked chitosan - polyether polymer network (semi-ipn) hydrogels. J Polym Sci Part A- Polym Chem 32(7):1213–1223. https://doi.org/10.1002/pola.1994.080320702
45. Masood N et al (2019) Silver nanoparticle impregnated chitosan-PEG hydrogel enhances wound healing in diabetes induced rabbits. Int J Pharm 559:23–36. https://doi.org/10.1016/j.ijpharm.2019.01.019
46. Thamer BM et al (2020) In situ preparation of novel porous nanocomposite hydrogel as effective adsorbent for the removal of cationic dyes from polluted water. Polymers 12(12). https://doi.org/10.3390/polym12123002
47. Chatterjee S, Lee MW, Woo SH (2010) Adsorption of congo red by chitosan hydrogel beads impregnated with carbon nanotubes. Bioresour Technol 101(6):1800–1806. https://doi.org/10.1016/j.biortech.2009.10.051
48. Fan C et al (2016) The stability of magnetic chitosan beads in the adsorption of Cu2+. RSC Adv 6(4):2678–2686. https://doi.org/10.1039/C5RA20943A
49. Fan C et al (2018) Evaluation of magnetic chitosan beads for adsorption of heavy metal ions. Sci Total Environ 627:1396–1403. https://doi.org/10.1016/j.scitotenv.2018.02.033
50. IM Kenawy et al (2019) Melamine grafted chitosan-montmorillonite nanocomposite for ferric ions adsorption: central composite design optimization study J Clean Prod 241.https://doi.org/10.1016/j.jclepro.2019.118189
51. Futalan CM et al (2012) Copper, nickel and lead adsorption from aqueous solution using chitosan-immobilized on bentonite in ternary system. Sustain Environ Res 22(6):345–355
52. Durán N et al (2016) Silver nanoparticles: a new view on mechanistic aspects on antimicrobial activity. Nanomed-Nanotechnol Biol Med 12(3):789–799. https://doi.org/10.1016/j.nano.2015.11.016
53. Roy A et al (2019) Green synthesis of silver nanoparticles: biomolecule-nanoparticle organizations targeting antimicrobial activity. RSC Adv 9(5):2673–2702. https://doi.org/10.1039/C8RA08982E
54. Feng QL et al (2000) A mechanistic study of the antibacterial effect of silver ions on Escherichia coli and Staphylococcus aureus. J Biomed Mater Res 52(4):662–668. https://doi.org/10.1002/1097-4636(20001215)52:4%3C662::AID-JBM10%3E3.0.CO;2-3
55. Kim JS et al (2007) Antimicrobial effects of silver nanoparticles. Nanomed-Nanotechnol Biol Med 3(1):95–101. https://doi.org/10.1016/j.nano.2006.12.001
56. Vertelov GK et al (2008) A versatile synthesis of highly bactericidal Myramistin (R) stabilized silver nanoparticles. Nanotechnology 19(35). https://doi.org/10.1088/0957-4484/19/35/355707
57. Piras CC, Mahon CS, Smith DK (2020) Self-assembled supramolecular hybrid hydrogel beads loaded with silver nanoparticles for antimicrobial applications. Chem Eur J 26(38):8452–8457. https://doi.org/10.1002/chem.202001349
58. Park S et al (2018) Disinfection of waterborne viruses using silver nanoparticle-decorated silica hybrid composites in water environments. Sci Total Environ 625:477–485. https://doi.org/10.1016/j.scitotenv.2017.12.318
59. Long YM et al (2017) Surface ligand controls silver ion release of nanosilver and its antibacterial activity against Escherichia coli. Int J Nanomed 12:3193–3206. https://doi.org/10.2147/IJN.S132327
60. Liu J, Hurt RH (2010) Ion release kinetics and particle persistence in aqueous nano-silver colloids. Environ Sci Technol 44(6):2169–2175. https://doi.org/10.1021/es9035557